4-15-2020

Imaging of membrane concentration polarization by NaCl using 23Na nuclear magnetic resonance

Masoumeh Zargar
Edith Cowan University

Ryuta Ujihara

Sarah J. Vogt

Johannes S. Vrouwenvelder

Einar O. Fridjonsson

See next page for additional authors

10.1016/j.memsci.2020.117868
Zargar, M., Ujihara, R., Vogt, S. J., Vrouwenvelder, J. S., Fridjonsson, E. O., & Johns, M. L. (2020). Imaging of membrane concentration polarization by NaCl using 23Na nuclear magnetic resonance. *Journal of Membrane Science, 600,* Article 117868. https://doi.org/10.1016/j.memsci.2020.117868

Imaging of Membrane Concentration Polarization by NaCl using ^{23}Na Nuclear Magnetic Resonance

Masoumeh Zargar[1, 2], Ryuta Ujihara[1], Sarah J. Vogt[1], Johannes S. Vrouwenvelder[3, 4], Einar O. Fridjonsson[1], Michael L. Johns[1]

[1] Department of Chemical Engineering, University of Western Australia, Crawley WA 6009, Australia
[2] School of Engineering, Edith Cowan University, Joondalup, WA 6027, Australia
[3] Biological and Environmental Sciences and Engineering Division, Water Desalination and Reuse Center, King Abdullah University of Science and Technology, Thuwal 23955-6900, Saudi Arabia
[4] Department of Biotechnology, Faculty of Applied Sciences, Delft University of Technology, Van der Maasweg 9, 2629 HZ Delft, The Netherlands.

Abstract

Forward osmosis (FO) and reverse osmosis (RO) membrane processes differ in their driving forces: osmotic pressure versus hydraulic pressure. Concentration polarization (CP) can adversely affect both performance and lifetime in such membrane systems. In order to mitigate against CP, the extent and severity of it need to be predicted more accurately through advanced online monitoring methodologies. Whilst a variety of monitoring techniques have been used to study the CP mechanism, there is still a pressing need to develop and apply non-invasive, *in situ* techniques able to produce quantitative, spatially resolved measurements of heterogeneous solute concentration in, and adjacent to, the membrane assembly as caused by the CP mechanism. To this end, ^{23}Na magnetic resonance imaging (MRI) is used to image the sodium ion concentration within, and near to, both FO and RO composite membranes for the first time; this is also coupled with ^{1}H MRI mapping of the corresponding water distribution. As such, it is possible to directly image salt accumulation due to CP processes during desalination. This was consistent with literature expectations and serves to confirm the suitability of ^{23}Na MRI as a novel non-invasive technique for CP studies.

Keywords:

Sodium; concentration polarization; magnetic resonance imaging; forward osmosis; reverse osmosis

1. Introduction

Forward osmosis (FO) is an emerging membrane-based technique which is being explored as a potential option for low cost desalination and wastewater treatment membranes. This osmotically-driven process comprises two steps: permeate from a saline feed solution (FS) initially transverses a semi-permeable membrane via osmosis to a concentrated draw solution (DS); this water is then recovered from the DS via the application of an additional separation process [1-3]. If the DS regeneration, which is energy-intensive, can be adequately managed, FO can potentially offer lower energy consumption compared to pressure-driven membrane processes such as reverse osmosis (RO), ultrafiltration, and nanofiltration that require significant hydraulic pressures to force water through the membranes. FO is also argued to offer lower fouling propensity (which is more reversible) and can be applied to a wide range of solutes and contaminants [1-5]. Similar to RO membranes, a significant limitation with respect to FO application is the occurrence of concentration polarization (CP). CP is the elevated concentration of either solutes or particles, relative to the bulk concentrations, either inside or on the surface of the membrane assembly. This serves to both reduce the osmotic driving force (and hence adversely affect membrane performance) and in the longer term, reduce membranes durability [6-8]. Local elevations in solute concentration can potentially result in local crystallization on the membrane surface; these also serve to change the concentration gradient of solutes across the membrane which usually serves to reduce the osmotic pressure driving force, and hence permeate flux declines [9-11]. The magnitude of the CP effect is reduced by increased cross-flow over the membrane surface and/or the application of turbulence promoters or spacers; these hydrodynamic effects are however significantly influenced by the geometry of the membrane assembly [8].

In general, CP in membranes has two forms: external concentration polarization (ECP), which happens on the outer surface of membranes and internal concentration polarization (ICP) that happens within the porous support layer of the membranes [11] – this is schematically shown in Figure 1. During FO, water permeates from the feed solution to the draw solution due to osmosis; the membrane configuration can either have the active membrane layer facing the feed solution (AL-FS) or the active membrane layer facing the draw solution (AL-DS); the latter is also referred to as pressure retarded osmosis (PRO). Both orientations are schematically shown in Figure 1. During FO in the AL-FS configuration (Figure 1(a)), water permeation results in ECP on the active side of the membrane and dilutive ICP within the membrane support layer; whilst FO in the AL-DS configuration (Figure 1(b)) results in ICP in the membrane support later and dilutive ECP on the external active membrane layer [12, 13]. In both configurations, the net osmotic force decreases hence reducing membrane performance [11, 12, 14]. ECP, as discussed above, can be reduced via cross-flow; however, ICP is much more challenging to control resulting in a potentially greater negative impact on membrane performance [15-18].

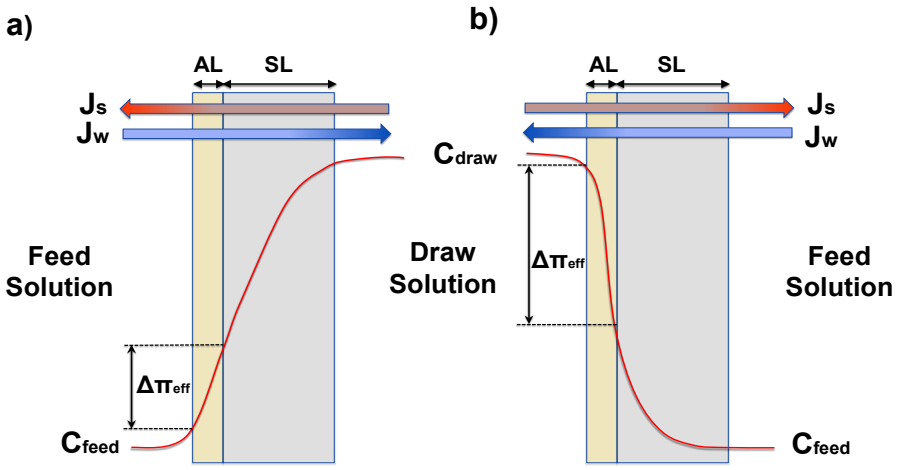

Fig.1 Schematic illustration of solute concentration profile and concentration polarization (CP) mechanism in the vicinity and within the support layer of a thin film composite (TFC) FO membrane configured in a) AL-FS mode, and b) PRO mode, where J_w is water flux, J_s is solute flux, $\Delta\pi_{eff}$ is the effective osmotic pressure difference, and C_{feed} and C_{draw} are the solute concentrations in the feed and draw solutions respectively [13].

A variety of measurement techniques have been applied to investigate CP in membranes [e.g. 19-22]. *In-situ* monitoring techniques that have been applied to evaluate CP in filtration membranes include light deflection methods (shadowgraphy and refractometry), both of which require optical access and some optical property (e.g. refractive index) to quantitatively depend on the solute concentration. Other CP analysis techniques include radioisotope labeling, electron diode array microscopy, and direct pressure measurement [19, 20, 23]. However, all these techniques have some limitations which make the *in-situ* accurate quantification of solute concentration difficult [19, 20]. For example, Vilker et al. [19] used shadowgraphy to predict bovine serum albumin (BSA) concentration profiles in a membrane polarization layer in the absence of gel/cake formation. Although their experimental BSA concentration results showed reasonably good agreement with theoretical predictions, their experimental BSA diffusivity values were one order of magnitude different from their theoretical predictions. Zhang and Ethier [23] measured the pressure distribution profile within a concentration polarization layer with the aid of a miniature sensor. Whilst innovative, the technique is inevitably invasive and potentially perturbs the polarization layer. In particular, measurements of any ICP are difficult. Hence, the application of a non-destructive, non-invasive approach that can directly quantify the spatial distribution of solute or colloidal material during CP on and in an active membrane is highly desirable.

Magnetic Resonance Imaging (MRI) is a versatile non-destructive technique that can be used to study the structural and transport properties of membranes [e.g., 24]. In conventional MRI, the signal detected reflects the proton (^{1}H) concentration; this signal can also be moderated by either longitudinal (T_1) or transversal (T_2) relaxation in order to reflect local confinement of the relevant fluid. Other contrast mechanisms include the use of chemical shift (to differentiate between oil and water for example) and diffusion or flow. In this broad context, MRI has been widely applied to monitor filtration membranes in terms of their structure,

fouling, and transport properties [e.g. 24-33]. This includes the use of low field bench-top MRI systems capable of imaging fouling development in RO desalination membranes [24, 27, 30]. Fouling and its effect on the local flow field have also been studied using MRI for multichannel hollow fiber membranes [25]. In the context of membrane CP, ^{1}H MRI has been used by Pope *et al*. to explore the accumulation of polarized layers adjacent to the membrane surface during cross-flow filtration of both colloidal silica material and oil-in-water emulsions [e.g., 26, 34, 35]. They used chemical shift selective micro-imaging to directly visualize the creation and development of oil polarization layers during the filtration of the oil-in-water emulsions, enabling determination of the oil layer thickness and spatially localized resistance [34] as well as the axial flowrate [35].

In the current work, a custom-built cross-flow planar membrane module was constructed which was compatible with high field MRI equipment. This was able to accommodate either a FO or RO membrane; the thicker RO membrane was used primarily for validation purposes. Both ^{1}H and ^{23}Na two-dimensional (2D) MRI were performed perpendicular to the membrane allowing both the water and NaCl concentration to be determined as a function of distance from, and into, the membrane at a spatial resolution of 10 μm. Imaging was thus performed on systems relevant to desalination, with images acquired mainly immediately after the cessation of cross-flow. The FO membranes were investigated in both AL-FS and AL-DS configurations. To the best of our knowledge, this is the first attempt to apply ^{23}Na MRI to directly measure NaCl concentration polarization in a membrane system.

2. Materials and Methods

FO membranes were purchased from HTI (Albany, OR, USA) and Porifera (Hayward, CA, USA) respectively and the thin film composite (TFC) RO membranes were obtained from Dow FILMTEC (Minneapolis, MN, USA). The HTI, Porifera and Filmtec membranes used were 115, 50, and 300 μm thick, respectively. The 2D membrane module used was an adaptation of the membrane fouling simulator used for early detection of membrane fouling [28, 29, 36]. This included two separate channels for delivery and removal of the feed and draw solutions respectively. The membrane was positioned between these channels, clamped in place mechanically and supported on both sides via two 28 mil (711 μm) thick spacers. The resultant module was made of PVC (delivering no NMR signal) and had inner flow chamber dimensions of 2×200×216 mm^3. Figure 2(a) presents a schematic of the module. Sodium chloride (99.7% purity, Chem-Supply, SA, Australia) and DI water (conductivity <1 μS/cm, Ibis Technology, WA, Australia) were used to prepare the feed (0.1 M NaCl) and draw (2 M NaCl) solutions.

High-resolution magnetic resonance images were obtained using a horizontal bore Bruker BioSpec MRI scanner (Figure 2(b)) with a magnetic field of 9.4 T and a dual radio-frequency (RF) coil (diameter of 154 mm) tuned to the ^{1}H (ω = 400.1 MHz) and ^{23}Na (ω = 105.8 MHz) resonance frequencies respectively. A maximum gradient strength of 0.33 T/m was used. Spin-echo 2D images (with an axial (z) slice thickness of 1 mm) and with an in-plane resolution of 0.01 mm (y) by 1 mm (x) for the RO membrane and 0.01 mm (y) by 1.7 mm (x)

for the FO membranes, were acquired separately using both ^{1}H and ^{23}Na detection. The membrane module was placed in the dual RF coil inside the magnet and connected to a flow line as schematically illustrated in Figure 2(c); in this configuration water at different salinities is simply flowed on either side of the membrane (the feed side (FS) and draw side (DS) respectively) in two discrete flow loops at flowrates of 1.08 L/h. ^{1}H images were used to determine the water content in, and adjacent, to the membranes, whilst ^{23}Na images were used to determine the respective salt distribution. The signal to noise ratio (SNR) of the ^{23}Na images is inevitable poorer [37] than that of the ^{1}H images. SNR is proportional to $\omega^{7/4}$ [38] meaning that an equivalent number of ^{23}Na nuclei delivers only 10 % of the SNR of ^{1}H nuclei. In our case, the density of ^{23}Na will also be significantly smaller. Nevertheless, it was possible to acquire a full 2D ^{23}Na image in 8 minutes with a *y*-direction spatial resolution of 10 microns. For both ^{1}H and ^{23}Na imaging, 8 signal averages were used. This is made possible via the use of a 9.4 T magnet and exploitation of the short T_1 of the ^{23}Na (less than 50 ms) meaning that a recycle time of only 200 ms could be used between ^{23}Na signal acquisitions; in the case of ^{1}H detection the recycle time was increased to 2 s. The T_2 of ^{23}Na in bulk solution was measured to be 25 ms using a standard CPMG pulse sequence; given an echo time of 2 ms, no significant T_2 relaxation weighting is expected in the acquired images for bulk solution ^{23}Na; greater T_2 relaxation is however possible in the membrane assembly itself as discussed below. For the case of ^{1}H signal detection (from the water content), the T_2 value was 2 s in the bulk and 42 ms in the membrane assembly; however, exchange of water molecules between the bulk and the membrane would have occurred over the measurement timeframe and hence these values thus need to be treated cautiously.

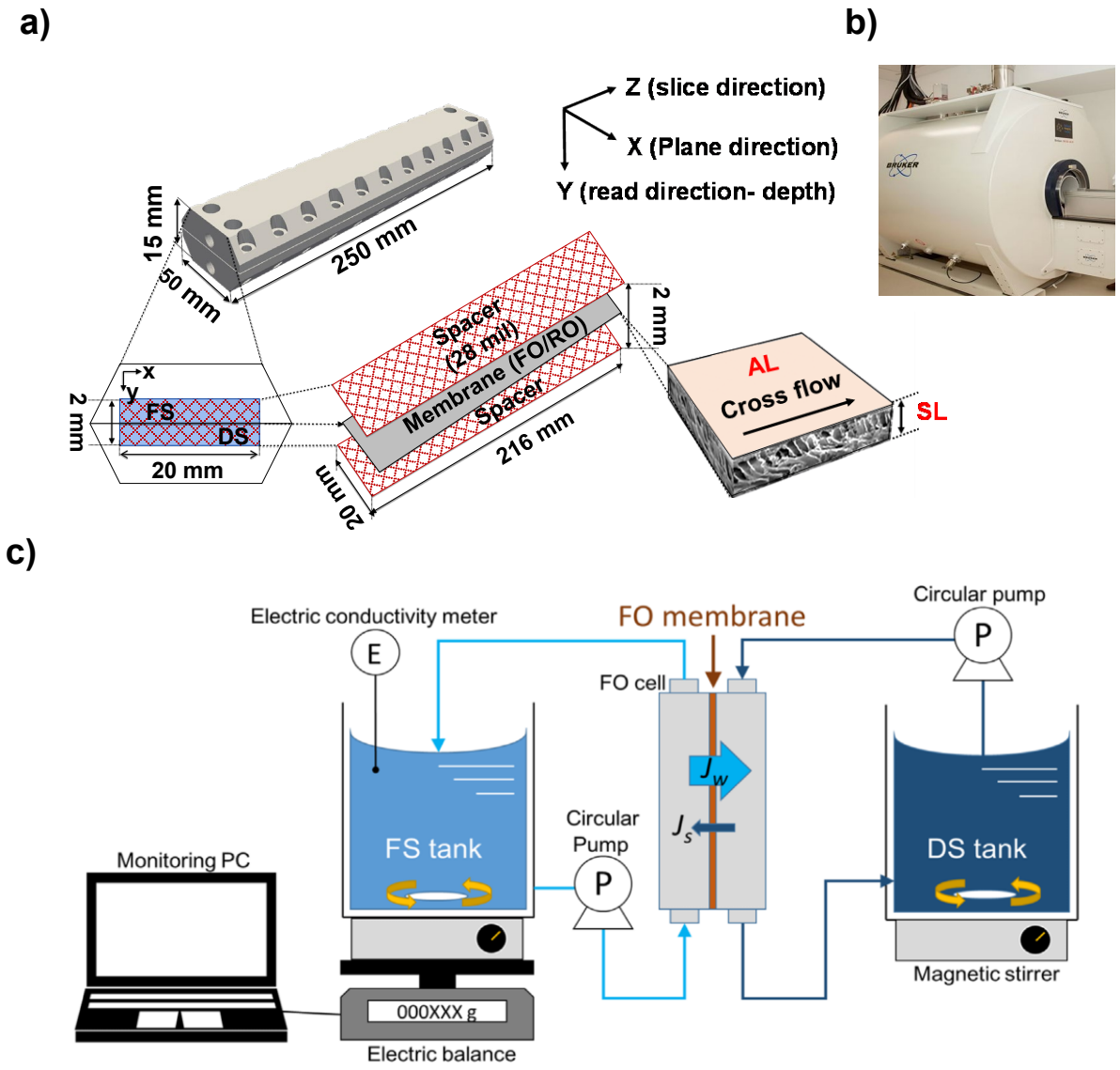

Fig. 2 a) The schematic illustration of a) the custom-made FO membrane fouling simulator cell, b) Bruker Biospec 9.4 T MRI animal imaging system, and c) the experimental setup.

1. Results and Discussion

Imaging was performed with the aforementioned FO or RO membranes individually sandwiched between two spacer sheets in the membrane cell (shown in Figure 2(a)). In all cases, brine solution at 2 M was present on one side of the membrane whilst dilute brine solution (0.1 M NaCl) was present on the other. Figure 3(a) and (b) show the ^{1}H and ^{23}Na MRI images for the 300 micron thick TFC-RO membrane in the Al-DS orientation. The image intensity indicates the concentration of ^{23}Na and ^{1}H (and hence water) respectively. As expected, water is evident on both sides of the membrane, whereas sodium is predominately evident on the feed side. The 2D ^{23}Na and ^{1}H images were averaged in the *x*-direction to produce the 1D ^{23}Na and ^{1}H *y*-direction profiles shown in Figure 3(c) and magnified in Figure

3(d). The presence of the spacers (which deliver no NMR signal) is reflected in the ^{1}H profile shape with elevated ^{1}H concentrations at either end. Elevated Na concentration within both the active and support membrane layers is immediately evident and there is some evidence (Figure 3(d) where the ^{23}Na signal exceeds that of the ^{1}H)) for elevated sodium concentration adjacent to the membrane and hence ECP. However, different regions of the membrane assembly have different microstructures and thus potentially different NMR T_2 relaxation properties [39] and hence minor variations in signal intensity need to be treated with caution. The active layer (AL) is dense while the support layer (SL) has a multi-layer, heterogeneous structure. The support layer in TFC membranes consists of a microporous polymer with a tighter skin on the top to support the AL and a fabric layer on the bottom with an open-pore structure. This is reflected in the ^{1}H profile where elevated signal is received from the bottom of the support structure. The results in Figure 3 confirm the ability of MRI to detect sodium in such, admittedly, thicker RO membrane systems; we now turn our attention to the detection of sodium in thinner FO membrane assemblies.

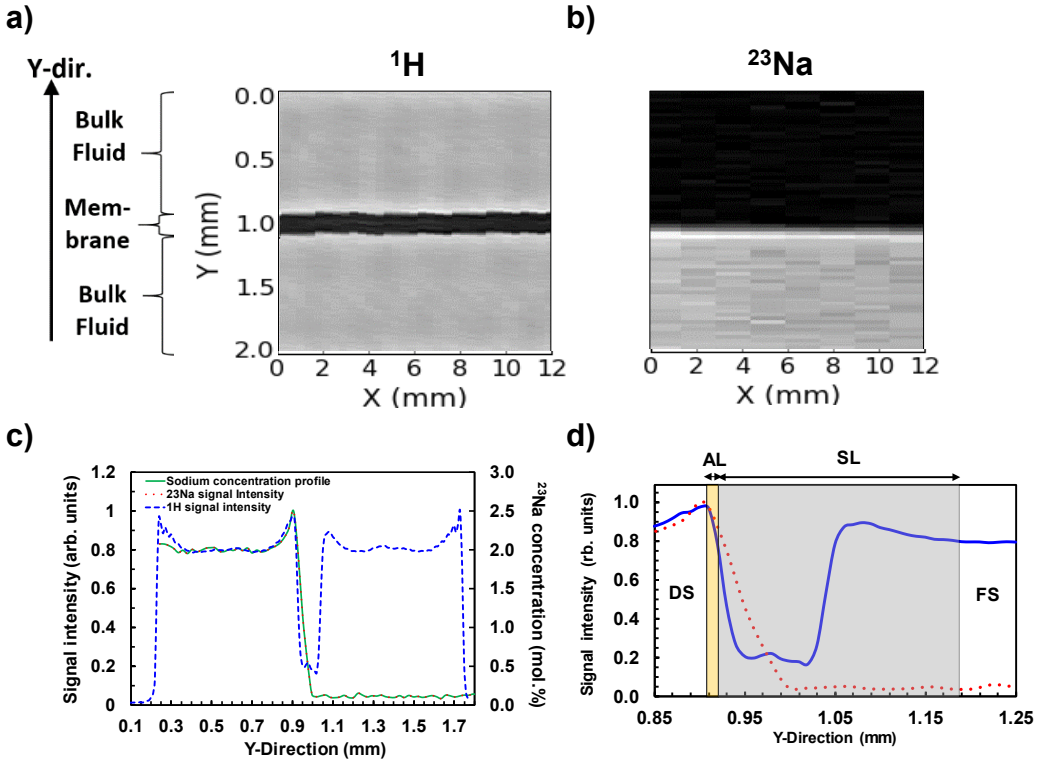

Fig. 3 a) ^{1}H 2D MRI and b) ^{23}Na 2D MRI of a flat sheet TFC-RO membrane module containing two spacers at the membrane feed and permeate side (0.01 mm (Y) by 1 mm (X) in-plane resolution), c) ^{1}H and ^{23}Na profiles of the membrane following averaging across the *x*-direction and d) a magnified profile of the membrane with the active and support layers (AL and SL) shown. The penetration of the Na signal into the support later is evident through the magnified profile presented in Figure 3 (d).

Figures 4(a) and (b) show 2D ^{1}H and ^{23}Na images of the HTI FO membrane in the AL-FS orientation in the membrane cell. The combined membrane active and support layers in this case have a thickness of 115 µm. This comparative thinness and hence flexibility of the membrane meant that a completely flat membrane profile was not possible, as is immediately evident in Figure 4(a and b). Similarly to Figure 3, the ^{23}Na and ^{1}H concentrations are averaged

across the *x*-direction resulting in Figure 4(c). In this case each y-axis profile was adjusted such that all the profiles lined up with the membrane in the same position. The ^{1}H profile is broadly consistent with Figure 3(c); the elevated apparent concentration adjacent to the membrane surface must reflect reduced signal relaxation in this region due to greater restricted diffusion of the water molecules in addition to the presence of the spacers on both sides of the membrane. The ^{23}Na profile shows a gradual reduction towards the outer edge of the draw solution side. The reason for this is unclear at present but could reflect the effect of spacer compression and system hydrodynamics. The membrane area is expanded in Figure 4(d) to evaluate the CP mechanism.

ECP is characterized by the mass transfer coefficient, *k*, which can be improved by increasing the cross-flow velocity or spacer design [8]. On the other hand, ICP is characterized via solute diffusivity in water, *D*, and the structural parameter of the membrane support layer, $S = \tau_m \cdot l_m/\varepsilon_m$, where τ_m, l_m, *and* ε_m are the support layer tortuosity, thickness, and porosity, respectively. In FO systems, a smaller value of *S* is more desirable as it leads to a smaller ICP and higher osmotic driving force [21]. Here, there is a significant accumulation of sodium within the membrane support structure (dilutive ICP) due to the relatively high structural parameter of this membrane (≈ 700 µm). Further, significant accumulation of sodium and hence concentrative ECP is present on the FS side of the membrane due to the boundary layer resistance to solute diffusion [40-42]. This data is broadly consistent with the expected profile shape as schematically shown in Figure 1 and as reported in the literature [42-45].

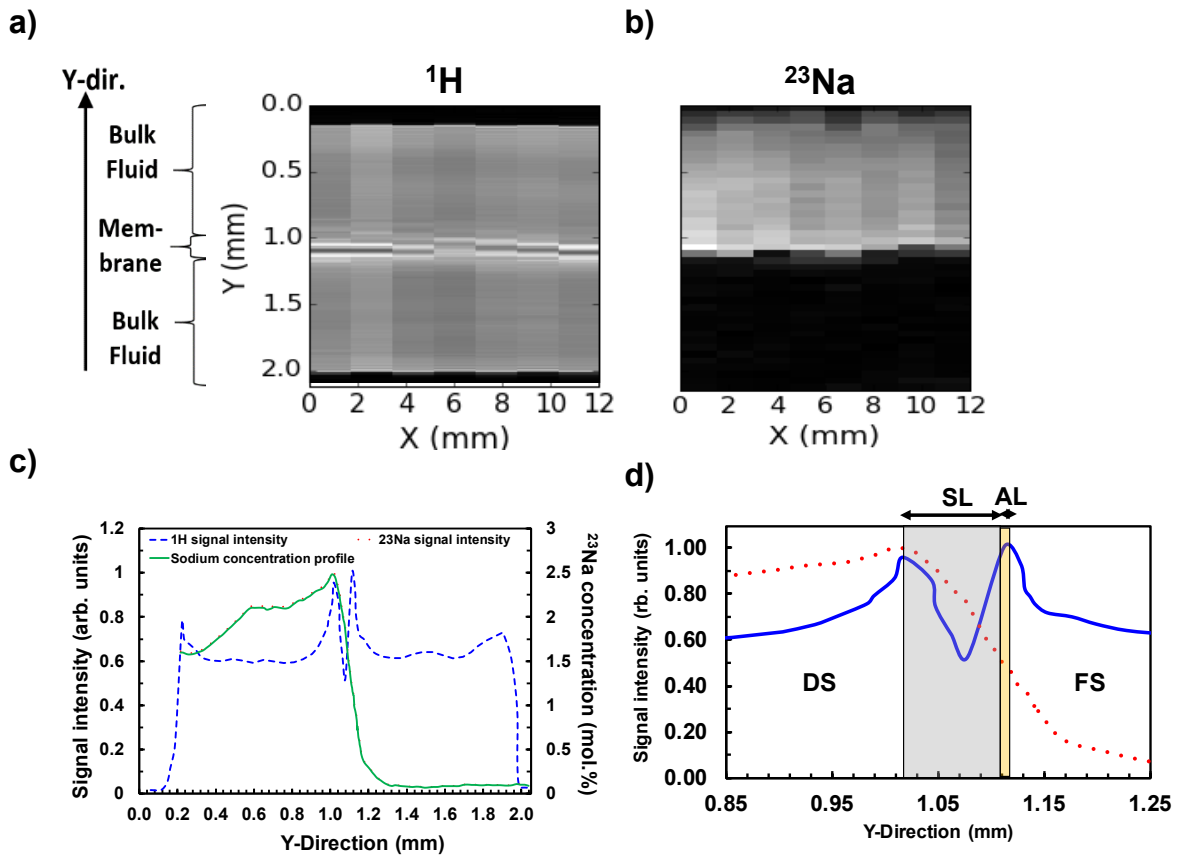

Fig. 4 a) 2D ^{1}H MRI b) 2D ^{23}Na MRI images of the FO membrane module sitting inside the module in a AL-FS configuration (with two spacers on the membrane feed and permeate side) with an in-plane resolution of 0.01 mm (y) by 1.7 mm (x), c) y-direction proton and sodium signal intensity profiles and sodium concentration in the whole channel and d) the profiles within the membrane showing the penetration of the Na signal into the support and active layers.

Next we turn our attention to the much more fragile Porifera FO membrane which is significantly thinner (50 µm) – an AL-DS orientation was used (as schematically shown in Figure 5(a)). In this case, ^{23}Na imaging was performed on the system with the FS flowing with a linear flow velocity corresponding to 1.08 L/h whilst the DS was stationary (but not contained with room for expansion due to being connected to the DS reservoir); a rapid imaging technique (Flash MRI imaging with an in-plane resolution of 25 µm [38, 46]) was applied enabling the 2D images to be acquired at an interval of 90 s. The time series of the resultant images are shown in Figure 5(b). Dilution of the DS salt concentration is evident over time as water migrates across the membrane under osmotic pressure differences – the kinetics of this are shown in Figure 5(c) by the red line, which presents the total ^{23}Na signal averaged across the whole image. Considering the channel and spacer dimensions as detailed in Figure 2(a) and Figure 5(b), a 3.6 ml volume is occupied by the feed and draw solutions on each side of the membrane. For the Porifera membrane with a calculated water flux of 15.7 LMH and a surface area of 43.2 cm^2, 1.9 ml of water permeates across the membrane every 100 s gradually diluting the DS. This dilution is shown by the blue crosses in Figure 5(c), which assumes a well-mixed system. This theoretical prediction is very consistent with the experimental data (red line in Figure 5(c)). This serves to prove that rapid imaging of the FO membrane filtration process is possible albeit not at a spatial resolution that enables any CP to be imaged.

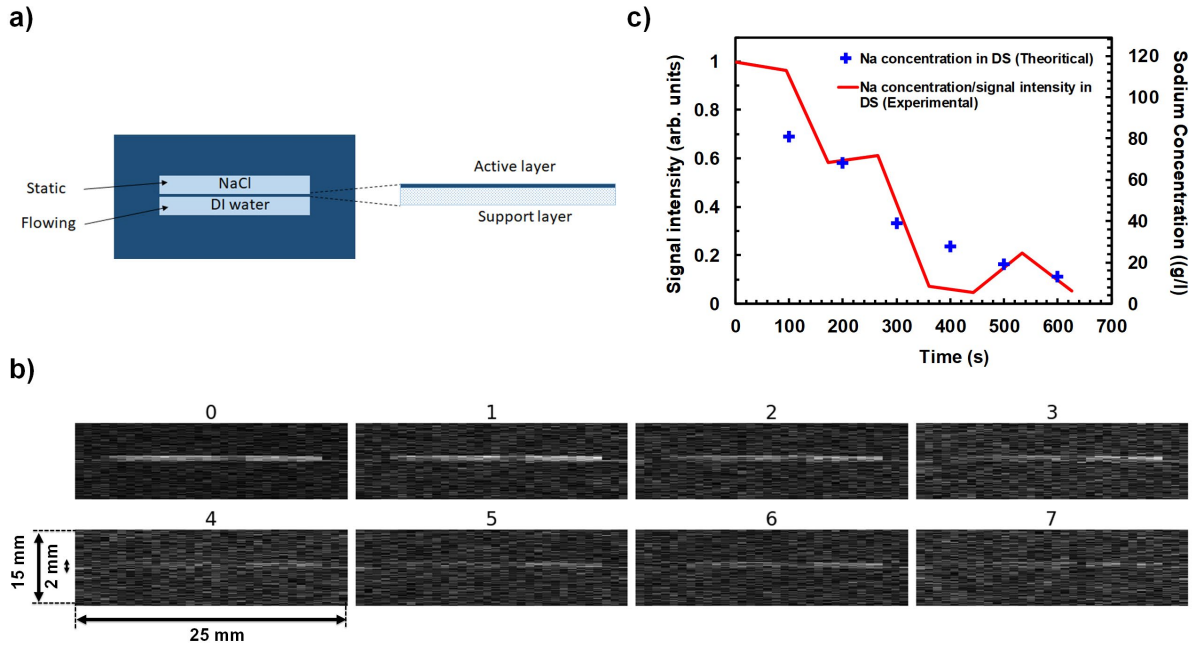

Fig. 5 a) Membrane configuration for Flash ^{23}Na MRI tests on the Porifera membrane operating with AL-DS mode under a dynamic flow condition, b) 2D Flash ^{23}Na MRI images of the whole channel at 90 s intervals and (c) temporal sodium concentration profile – as measured and as predicted from theory.

The qualitative consistency of our MRI results with theoretical predictions and literature indicates the unique insights possible with ^{23}Na MRI regards membrane concentration polarization. In particular, the use of ^{23}Na NMR allows the salt accumulation to be directly imaged both within and adjacent to the membrane assembly. Future work will focus on rendering the measurement more quantitative by a detailed consideration of T_2 relaxation processes; this is complicated by the effect of restricted diffusion in and adjacent to the membrane surface, an effect which was immediately obvious for the ^{1}H profiles in Figure 4. To this end, we will determine the diffusion coefficient of both water and Na using NMR pulsed field gradient (PFG) techniques; this will be spatially resolved in combination with MRI.

2. Conclusion

An RO and two FO membranes were tested individually in a custom-made effectively 2D desalination unit in AL-FS or AL-DS modes with both proton and sodium MRI imaging successfully applied to determine the water and Na ion concentrations both in and adjacent to the membrane assembly. Imaging was performed immediately after the cessation of cross-flow. Concentration polarization was evident in both membrane structures via the accumulation of sodium in the support layer of the membrane assembly. Comparatively rapid ^{23}Na MRI detection was also shown to be able to determine the dilution of a static draw solution in a dynamic FO scenario, the rate of which was consistent with expected membrane performance. These proof of concept results point to the significant potential of ^{23}Na MRI to provide a unique insight into concentration polarization processes occurring during desalination.

Acknowledgements

The authors acknowledge the facilities and scientific and technical assistance of the National Imaging Facility, a National Collaborative Research Infrastructure Strategy (NCRIS) capability, at the Centre for Microscopy, Characterisation and Analysis, The University of Western Australia. Funding from the Australian Research Council, the Forrest Research Foundation (for R. Ujihara) and the King Abdullah University of Science and Technology (KAUST) is gratefully acknowledged.

References

[1] Y. Hartanto, M. Zargar, H. Wang, B. Jin, S. Dai, Thermoresponsive Acidic Microgels as Functional Draw Agents for Forward Osmosis Desalination, Environmental Science & Technology 50(8) (2016) 4221-4228.

[2] N. Ma, J. Wei, S. Qi, Y. Zhao, Y. Gao, C.Y. Tang, Nanocomposite substrates for controlling internal concentration polarization in forward osmosis membranes, Journal of Membrane Science 441 (2013) 54-62.

[3] H. Rabiee, B. Jin, S. Yun, S. Dai, O_2/N_2-responsive microgels as functional draw agents for gas-triggering forward osmosis desalination, Journal of Membrane Science (2019) 117584.

[4] S. Zou, M. Qin, Z. He, Tackle reverse solute flux in forward osmosis towards sustainable water recovery: reduction and perspectives, Water Research 149 (2019) 362-374.

[5] Y. Hartanto, M. Zargar, X. Cui, B. Jin, S. Dai, Non-ionic copolymer microgels as high-performance draw materials for forward osmosis desalination, Journal of Membrane Science, 572 (2019) 480-488.

[6] A. Matin, F. Rahman, H.Z. Shafi, S.M. Zubair, Scaling of reverse osmosis membranes used in water desalination: Phenomena, impact, and control; future directions, Desalination 455 (2019) 135-157.

[7] H.J. Oh, Y.K. Choung, S. Lee, J.S. Choi, T.M. Hwang, J.H. Kim, Scale formation in reverse osmosis desalination: model development, Desalination 238(1) (2009) 333-346.

[8] M. Zargar, Jin, B., Dai, S., Development and application of reverse osmosis for separation, in: K.H.J.M. Dickson (Ed.), Membrane Processing for Dairy Ingredient Separation, Wiley2015.

[9] I. Sutzkover, D. Hasson, R. Semiat, Simple technique for measuring the concentration polarization level in a reverse osmosis system, Desalination 131(1) (2000) 117-127.

[10] M. Zargar, Y. Hartanto, B. Jin, S. Dai, Understanding functionalized silica nanoparticles incorporation in thin film composite membranes: Interactions and desalination performance, Journal of Membrane Science, 521 (2017) 53-64.

[11] A. Tiraferri, N.Y. Yip, A.P. Straub, S. Romero-Vargas Castrillon, M. Elimelech, A method for the simultaneous determination of transport and structural parameters of forward osmosis membranes, Journal of Membrane Science 444 (2013) 523-538.

[12] H. Zhang, S. Cheng, F. Yang, Use of a spacer to mitigate concentration polarization during forward osmosis process, Desalination 347 (2014) 112-119.

[13] S. Zhao, L. Zou, Relating solution physicochemical properties to internal concentration polarization in forward osmosis, Journal of Membrane Science 379(1) (2011) 459-467.

[14] X. Song, A. Prince, Relating Water/Solute Permeability Coefficients to the Performance of Thin-Film Nanofiber Composite Forward Osmosis Membrane, 2016.

[15] C.Y. Tang, Q. She, W.C.L. Lay, R. Wang, A.G. Fane, Coupled effects of internal concentration polarization and fouling on flux behavior of forward osmosis membranes during humic acid filtration, Journal of Membrane Science 354(1) (2010) 123-133.

[16] W.C.L. Lay, J. Zhang, C. Tang, R. Wang, Y. Liu, A.G. Fane, Factors affecting flux performance of forward osmosis systems, Journal of Membrane Science 394-395 (2012) 151-168.

[17] J.R. McCutcheon, M. Elimelech, Influence of concentrative and dilutive internal concentration polarization on flux behavior in forward osmosis, Journal of Membrane Science 284(1) (2006) 237-247.

[18] Y. Gao, Y.N. Wang, W. Li, C.Y. Tang, Characterization of internal and external concentration polarizations during forward osmosis processes, Desalination 338 (2014) 65-73.

[19] V.L. Vilker, C.K. Colton, K.A. Smith, Concentration polarization in protein ultrafiltration. Part I: An optical shadowgraph technique for measuring concenration profiles near a solution-membrane interface, AIChE Journal 27(4) (1981) 632-636.

[20] J.C. Chen, Q. Li, M. Elimelech, In situ monitoring techniques for concentration polarization and fouling phenomena in membrane filtration, Advances in Colloid and Interface Science 107(2) (2004) 83-108.

[21] L.M. Gowman, C. Ross Ethier, Concentration and concentration gradient measurements in an ultrafiltration concentration polarization layer Part II: Application to hyaluronan, Journal of Membrane Science 131(1) (1997) 107-123.

[22] F. Arndt, U. Roth, H. Nirschl, S. Schütz, G. Guthausen, New insights into sodium alginate fouling of ceramic hollow fiber membranes by NMR imaging, AIChE Journal 62(7) (2016) 2459-2467.

[23] W. Zhang, C.R. Ethier, Direct pressure measurements in a hyaluronan ultrafiltration concentration polarization layer, Colloids and Surfaces A: Physicochemical and Engineering Aspects 180(1) (2001) 63-73.

[24] E.O. Fridjonsson, S.J. Vogt, J.S. Vrouwenvelder, M.L. Johns, Early non-destructive biofouling detection in spiral wound RO membranes using a mobile earth′s field NMR, Journal of Membrane Science 489 (2015) 227-236.

[25] S. Schuhmann, J.W. Simkins, N. Schork, S.L. Codd, J.D. Seymour, M. Heijnen, F. Saravia, H. Horn, H. Nirschl, G. Guthausen, Characterization and quantification of structure and flow in multichannel polymer membranes by MRI, Journal of Membrane Science 570-571 (2019) 472-480.

[26] D. Airey, S. Yao, J. Wu, V. Chen, A.G. Fane, J.M. Pope, An investigation of concentration polarization phenomena in membrane filtration of colloidal silica suspensions by NMR micro-imaging, Journal of Membrane Science 145(2) (1998) 145-158.

[27] R. Ujihara, E. Fridjonsson, N. W Bristow, S. Vogt, S. Bucs, J.S. Vrouwenvelder, M. Johns, Earth's field MRI for the non-invasive detection of fouling in spiral-wound membrane modules in pressure vessels during operation, 2018.

[28] D.A. Graf von der Schulenburg, J.S. Vrouwenvelder, S.A. Creber, M.C.M. van Loosdrecht, M.L. Johns, Nuclear magnetic resonance microscopy studies of membrane biofouling, Journal of Membrane Science 323(1) (2008) 37-44.

[29] S.A. Creber, J.S. Vrouwenvelder, M.C.M. van Loosdrecht, M.L. Johns, Chemical cleaning of biofouling in reverse osmosis membranes evaluated using magnetic resonance imaging, Journal of Membrane Science 362(1) (2010) 202-210.

[30] X. Yang, E.O. Fridjonsson, M.L. Johns, R. Wang, A.G. Fane, A non-invasive study of flow dynamics in membrane distillation hollow fiber modules using low-field nuclear magnetic resonance imaging (MRI), Journal of Membrane Science 451 (2014) 46-54.

[31] N. Schork, S. Schuhmann, F. Arndt, S. Schütz, G. Guthausen, H. Nirschl, MRI investigations of filtration: Fouling and cleaning processes, Microporous and Mesoporous Materials 269 (2018) 60-64.

[32] S. Schuhmann, N. Schork, K. Beller, H. Nirschl, T. Oerther, G. Guthausen, In-situ characterization of deposits in ceramic hollow fiber membranes by compressed sensing RARE-MRI, AIChE Journal 64(11) (2018) 4039-4046.

[33] F. Arndt, S. Schuhmann, G. Guthausen, S. Schütz, H. Nirschl, In situ MRI of alginate fouling and flow in ceramic hollow fiber membranes, Journal of Membrane Science 524 (2017) 691-699.

[34] J.M. Pope, S. Yao, A.G. Fane, Quantitative measurements of the concentration polarisation layer thickness in membrane filtration of oil-water emulsions using NMR micro-imaging, Journal of Membrane Science 118(2) (1996) 247-257.

[35] S. Yao, A.G. Fane, J.M. Pope, An investigation of the fluidity of concentration polarisation layers in crossflow membrane filtration of an oil-water emulsion using chemical shift selective flow imaging, Magnetic Resonance Imaging 15(2) (1997) 235-242.

[36] J.S. Vrouwenvelder, J.A.M. van Paassen, L.P. Wessels, A.F. van Dam, S.M. Bakker, The Membrane Fouling Simulator: A practical tool for fouling prediction and control, Journal of Membrane Science 281(1) (2006) 316-324.

[37] N.K. Bangerter, G.J. Tarbox, M.D. Taylor, J.D. Kaggie, Quantitative sodium magnetic resonance imaging of cartilage, muscle, and tendon, Quant Imaging Med Surg 6(6) (2016) 699-714.

[38] P.T. Callaghan, Principles of Nuclear Magnetic Resonance Microscopy, Clarendon Press1993.

[39] Y. Talmon, L. Shtirberg, W. Harneit, O.Y. Rogozhnikova, V. Tormyshev, A. Blank, Molecular diffusion in porous media by PGSE ESR, Physical Chemistry Chemical Physics 12(23) (2010) 5998-6007.

[40] S.F. Pan, Y. Dong, Y.M. Zheng, L.B. Zhong, Z.H. Yuan, Self-sustained hydrophilic nanofiber thin film composite forward osmosis membranes: Preparation, characterization and application for simulated antibiotic wastewater treatment, Journal of Membrane Science 523 (2017) 205-215.

[41] J. Ren, J.R. McCutcheon, A new commercial thin film composite membrane for forward osmosis, Desalination 343 (2014) 187-193.

[42] A. Deshmukh, N.Y. Yip, S. Lin, M. Elimelech, Desalination by forward osmosis: Identifying performance limiting parameters through module-scale modeling, Journal of Membrane Science 491 (2015) 159-167.

[43] M. Darwish, H. Abdulrahim, A. Hassan, A.N. Mabrouk, A. Sharif, The forward osmosis and desalination, 2014.

[44] C.H. Tan, H.Y. Ng, Revised external and internal concentration polarization models to improve flux prediction in forward osmosis process, Desalination 309 (2013) 125-140.

[45] X. Wang, V. Chang, C. Y. Tang, Osmotic membrane bioreactor (OMBR) technology for wastewater treatment and reclamation: Advances, challenges, and prospects for the future, 2016.

[46] A. Haase, J. Frahm, D. Matthaei, W. Hanicke, K.D. Merboldt, FLASH imaging. Rapid NMR imaging using low flip-angle pulses, Journal of Magnetic Resonance 67(2) (1986) 258-266.